

SUPPORTING INFORMATION

Solvatomorphic Diversity Dictates the Stability and Solubility of Metal–organic Polyhedra

Ankit K. Yadav,^a Andrzej Gładysiak,^{a*} Emma H. Wolpert,^b Alex M. Ganose,^b Bronson Samel-Garloff,^c Dipankar Koley,^c Kim E. Jelfs,^b and Kyriakos C. Stylianou^{a*}

^a *Materials Discovery Laboratory (MaD Lab), Department of Chemistry, Oregon State University, Corvallis, OR 97331, United States.*

^b *Department of Chemistry, Molecular Sciences Research Hub, Imperial College London, White City Campus, 82 Wood Lane, W12 0BZ, United Kingdom.*

^c *Department of Chemistry, Oregon State University, Corvallis, OR 97331, United States.*

Email: andrzej.gladysiak@oregonstate.edu; kyriakos.stylianou@oregonstate.edu

Experimental

Materials. All the chemicals used in this study were purchased from Millipore Sigma, Sigma Aldrich, and Tokyo Chemical Industry, or Fisher, and used as received.

Synthesis of BVR-105. A glass vial was charged with 8 mg (0.02 mmol) of $\text{Mo}_2(\text{OAc})_4$, 35 mg (0.20 mmol) of $\text{H}_2\text{Iso-NH}_2$, 1 mL of anhydrous DMF, and 1 mL of anhydrous MeOH. Without any vigorous shaking, the mixture was heated at 120 °C for 48 h with a 2 °C/min ramping up and a 0.2 °C/min ramping down rates. Yellow, prism-shaped single crystals were isolated from the mother liquor upon cooling to room temperature.

Synthesis of BVR-106. A glass vial was charged with 17 mg (0.04 mmol) of $\text{Mo}_2(\text{OAc})_4$, 35 mg (0.20 mmol) of $\text{H}_2\text{Iso-NH}_2$, 1 mL of anhydrous DMF, and 1 mL of anhydrous MeOH. Without any vigorous shaking, the mixture was heated at 120 °C for 48 h with a 2 °C/min ramping up and a 0.2 °C/min ramping down rates. A mixture of BVR-105 and a few yellow, hexagonal-shaped single crystals of BVR-106 was isolated from the mother liquor upon cooling to room temperature and leaving it on the bench for at least one week at room temperature.

Synthesis of BVR-107. A glass vial was charged with 8 mg (0.02 mmol) of $\text{Mo}_2(\text{OAc})_4$, 35 mg (0.20 mmol) of $\text{H}_2\text{Iso-NH}_2$, 1 mL of anhydrous DMA, and 1 mL of anhydrous MeOH. Without any vigorous shaking, the mixture was heated at 120 °C for 48 h with a 2 °C/min ramping up and a 0.2 °C/min ramping down rates. Yellow, plate-shaped-single crystals were isolated from the mother liquor upon cooling to room temperature.

Synthesis of BVR-108 and BVR-109. A glass vial was charged with 8 mg (0.02 mmol) of $\text{Mo}_2(\text{OAc})_4$, 35 mg (0.20 mmol) of $\text{H}_2\text{Iso-NH}_2$, 1 mL of DEF, and 1 mL of anhydrous MeOH. Without any vigorous shaking, the mixture was heated at 120 °C for 48 h with a 2 °C/min ramping up and a 0.2 °C/min ramping down rates. A mixture of deep yellow, prism-shaped single crystals of BVR-108 and pale yellow, plate-shaped single crystals of BVR-109 was isolated from the mother liquor upon cooling to room temperature. Within that mixture, the contribution of BVR-109 to the total number of crystals was estimated from visible-light microscopy photographs by counting the crystals of the same habit and color.

Separation of BVR-108 and BVR-109. In the reaction vessel containing the mother liquor and the crystals of BVR-108 and BVR-109, the mother liquor was removed and replaced with fresh

DEF. When the vessel was shaken vigorously and left on the bench, it was observed that the crystals of BVR-109 settled at the bottom more rapidly than those of BVR-108. The still-floating crystals of BVR-108 were then removed from the vessel using a pipette. Subsequently, a fresh portion of DEF was introduced into the vessel, and the procedure was repeated iteratively. Phase-pure BVR-108 and BVR-109 were separately filtered and dried.

Single-crystal X-ray diffraction. Suitable crystals were selected and mounted onto a XtaLAB Synergy, Dualflex, HyPix 4-circle diffractometer. The crystals were kept at *ca.* 150 K during data collection. Using Olex2,¹ the structures were solved with the SHELXT structure solution program using Intrinsic Phasing,² and refined with the SHELXL refinement package using Least Squares minimization.³ Electron density in the structural voids was accounted for with Olex2 using the Solvent Mask algorithm analogous to Platon Squeeze (radius = 1.2 Å, truncation = 1.2 Å).⁴ The integral of the electron density was used to estimate the number of DMF, DMA, or DEF molecules disordered in the voids. This interpretation, as undertaken previously by other authors,⁵ was allowed by the full completeness of the reflection data.⁴

Crystal structure refinement of BVR-105. A half of the Mo(V)-MOP molecule, six dma⁺ cations, and one DMF molecule were modeled within the asymmetric unit (ASU). The integral electron density of 459.9 e⁻ per formula unit was interpreted as originating from 11.5 disordered DMF molecules (40 e⁻ each). Therefore, the number of DMF molecules per formula unit amounted to 2 (ordered) + 11.5 (disordered) = 13.5.

Crystal structure refinement of BVR-106. The structure was found to be slightly affected by merohedral twinning [twin law = (0, -1, 0, -1, 0, 0, 0, 0, -1), fractional volume contribution of the twin component = 0.046], and heavily affected by disorder about the six-fold axis. The atoms C12, C33, H33, and N31 were refined with full occupancy, while all the other atoms were refined with half occupancy and the SHELXL command `PART -1`. Consequently, the ASU comprised of one sixth of the Mo(V)-MOP molecule nearly all of which had the occupancy one half, as well as one dma⁺ cation with half occupancy, therefore $Z' = 1/12$, $Z = 1$. The integral electron density of 495.1 e⁻ per formula unit was interpreted as originating from 6 disordered dma⁺ cations (27 e⁻ each) and 8.3 disordered DMF molecules (40 e⁻ each).

Crystal structure refinement of BVR-107. One fourth of the Mo(V)-MOP molecule and two and a half dma⁺ cations were modeled within the ASU. A portion of the Iso-NH₂²⁻ ligand (atoms C36,

H36, C37, C38, H38, N31, H31A, and H31B) was found to be disordered about a two-fold axis. The integral electron density of 582.7 e⁻ per formula unit was interpreted as originating from 2 disordered dma⁺ cations (27 e⁻ each) and 11 disordered DMA molecules (48 e⁻ each).

Crystal structure refinement of BVR-108. A half of the Mo(V)-MOP molecule and six dea⁺ cations were modeled within the ASU. The integral electron density of 530.8 e⁻ per formula unit was interpreted as originating from 9.5 disordered DEF molecules (56 e⁻ each).

Crystal structure refinement of BVR-109. The structure was affected by non-merohedral twinning [twin law = (0.5067, -0.2955, 0.4936, -0.0017, -0.9998, -0.0002, 1.5027, -0.2953, -0.5071), or 179.9848° rotation the reciprocal-space vector (0.7082 -0.0009 0.7060), fractional volume contribution of the twin component = 0.5040(15)], and refined using the SHELXL command `HKLF 5`. Two halves of the Mo(V)-MOP molecule and six dea⁺ cations were modeled within the ASU. The integral electron density of 1,109.4 e⁻ per formula unit was interpreted as originating from 6 disordered dea⁺ cations (43 e⁻ each) and 15.2 disordered DEF molecules (56 e⁻ each).

Powder X-ray diffraction. Fresh crystals of Mo(V)-MOPs and small portions of amide solvents were ground using a mortar and pestle. BVR-105 was ground in the presence of DMF; BVR-107 was ground in the presence of DMA; BVR-108 was ground in the presence of DEF, and so was BVR-109. The resulting slurries were introduced into borosilicate glass capillaries (1 mm in diameter for BVR-105, BVR-107, and BVR-108, and 0.5 mm in diameter for BVR-109), which were then mounted onto a Rigaku SmartLab diffractometer equipped with a copper-anode X-ray tube and a 1D line detector. PXRD patterns were recorded in transmission mode at ambient temperature and served as input for Pawley refinements, which were performed using TOPAS-Academic Version 7.⁶ In another measurement campaign, dried powders of Mo(V)-MOPs were placed on flat silicon-wafer sample holders, which were then mounted onto a MiniFlex benchtop diffractometer equipped with a copper-anode X-ray tube and a 1D line detector. PXRD patterns were recorded in reflection mode at ambient temperature and used for qualitative comparison with other PXRD patterns.

X-ray photoelectron spectroscopy. A copper double-sided tape (TED PELLA, INC.) was mounted on a typical stainless steel SPECS holder for XPS. Using a fast entry lock (base pressure ~1 × 10⁻⁸ mbar), the Mo(V)-MOP powder was loaded into the ultrahigh vacuum (UHV) system

after being compressed onto the tape. A near-ambient pressure (NAP) system, specially designed by SPECS Surface Nano Analysis GmbH, was used. An ultrahigh UHV manipulator ($<2 \times 10^{-10}$ mbar) was equipped with the system to perform standard XPS in UHV, and a near ambient pressure (NAP) cell (fit for NAP-XPS) could be moved into the analysis chamber. It was possible to pressurize the NAP cell to approximately 10 mbar while keeping the surrounding chamber vacuum at 1×10^{-9} mbar. Using monochromatized Al K α radiation ($h\nu = 1486.6$ eV; 50 W, and 15 kV), XPS was conducted at room temperature on the C 1s, O 1s, and Mo 3d core levels and valence-band. Using normal emission, the electron analyzer pass energy was set to 69 eV.

Fourier-transform infrared spectroscopy. FT-IR spectra were recorded using a PerkinElmer Spectrum Two attenuated total reflection analyzer.

Ultraviolet-visible spectroscopy. UV-Vis spectra were collected using PerkinElmer UV/VIS/NIR spectrometer Lambda 1050+ between 200 and 800 nm wavelength.

Nuclear magnetic resonance spectroscopy. For each sample, 2 mg of dry powder were dissolved in 650 μ L of D₂O, and the solution was poured into a standard NMR tube. NMR spectra were recorded at 25 °C using a Bruker Ascend 500 MHz 4-channel NMR spectrometer equipped with a 5 mm BBOF probe.

Porosity assessment. Dry powders were outgassed at 120 °C for 12 h. N₂ and H₂ adsorption isotherms at 77 K, and CO₂ adsorption isotherms at 298 K were recorded using the 3Flex sorption analyzer. Surface areas were determined using the Brunauer-Emmett-Teller (BET) method.

Thermogravimetric analysis. TGA curves were recorded on a TA Instruments STD Q600 analyzer using a temperature ramp of 10 °C/min in an argon environment with a flow rate of 100 mL/min.

BVR-105 synthesis kinetics. A series of glass vials was prepared. Each glass vial was charged with 8 mg (0.02 mmol) of Mo₂(OAc)₄, 35 mg (0.20 mmol) of H₂Iso-NH₂, and 2 mL of anhydrous DMF, with no addition of MeOH. Without any vigorous shaking, the vials were placed in an oven pre-heated to 120 °C and kept at this temperature for either 2, 4, 6, 8, 16, 24, or 48 h. After a given time elapsed, each vial was removed from the oven, photographed, and UV-vis spectra of its liquid content were recorded. The reaction mixture that was not subjected to high temperature (denoted as “0 h”) was investigated as a reference.

BVR-107 synthesis kinetics. A series of glass vials was prepared. Each glass vial was charged with 8 mg (0.02 mmol) of $\text{Mo}_2(\text{OAc})_4$, 35 mg (0.20 mmol) of $\text{H}_2\text{Iso-NH}_2$, and 2 mL of anhydrous DMA, with no addition of MeOH. Without any vigorous shaking, the vials were placed in an oven pre-heated to 120 °C and kept at this temperature for either 2, 4, 6, 8, 24, or 48 h. After a given time elapsed, each vial was removed from the oven, photographed, and UV-vis and FT-IR spectra of its liquid content were recorded. The reaction mixture that was not subjected to high temperature (denoted as “0 h”) was investigated as a reference.

BVR-108 synthesis kinetics. A series of glass vials was prepared. Each glass vial was charged with 8 mg (0.02 mmol) of $\text{Mo}_2(\text{OAc})_4$, 35 mg (0.20 mmol) of $\text{H}_2\text{Iso-NH}_2$, and 2 mL of anhydrous DEF, with no addition of MeOH. Without any vigorous shaking, the vials were placed in an oven pre-heated to 120 °C and kept at this temperature for either 2, 4, 6, 8, 16, 24, or 48 h. After a given time elapsed, each vial was removed from the oven, photographed, and UV-vis and FT-IR spectra of its liquid content were recorded. The reaction mixture that was not subjected to high temperature (denoted as “0 h”) was investigated as a reference.

Solubility measurements. Three biphasic systems composed of the saturated MOP aqueous solution in dynamic equilibrium with non-dissolved powder were prepared by mixing and sonicating for 4 h: (i) 5 mg of BVR-107 in 1 mL of deionized water, (ii) 15 mg of BVR-108 in 1 mL of deionized water, and (iii) 15 mg of BVR-109 in 1 mL of deionized water. To remove excess insoluble MOP crystals, the systems were filtered through a 0.45 μm syringe filter. The amount of molybdenum in each saturated solution was determined in triplicate with inductively coupled plasma optical emission spectroscopy (ICP-OES), and the average value, expressed in grams per liter, was interpreted as MOP solubility.

Electrical conductivity measurements. Solutions of known molar concentrations were prepared by dissolving either of the BVR-107, BVR-108, and BVR-109 powders in deionized water. Electrical conductivities of the solutions were measured at room temperature with an Oakton CON 6+ handheld conductivity meter. Molar conductivities were calculated by dividing the conductivities by the respective molar concentrations. Values of limiting molar conductivity and $\text{p}K_a$ were calculated by fitting the concentration and molar conductivity data to Ostwald’s dilution law.

DFT calculations. During crystallographic analysis of BVR-106, BVR-107, and BVR-109 the positions of the cations were unable to be fully resolved. Extra cations were added to the solved structure to balance the charge of the system and make them stoichiometrically equivalent. To place the cations in chemically sensible positions, we examined where residual electronic density was found in the SCXRD analysis and placed cations accordingly to achieve charge neutrality. For BVR-106, BVR-107, and BVR-109 this meant adding 6, 4, and 6 cations per molecular unit respectively.

Density functional theory calculations were performed using the Vienna *Ab initio* Simulation Package (VASP).⁷ A plane wave basis set with an energy cutoff of 680 eV and a $1 \times 1 \times 1$ Γ -centred k-point mesh were employed. Calculations were performed with the Perdew-Burke-Ernzerhof (PBE) exchange–correlation functional⁸ with dispersion interactions included via Grimme's D3 dispersion correction.⁹ To account for the self-interaction error inherent to semi-local density functionals, we employed the empirical +U correction of Dudarev *et al.*,¹⁰ which amounts to an on-site correction of the Coulomb interaction on the localized Mo d orbitals ($U=4.38$).¹¹ For each structure, both ferromagnetic and antiferromagnetic orderings were trialed, with the latter found to be marginally lower in energy in all cases. Structures were relaxed until the forces on all atoms totaled less than 2 meV/Å.

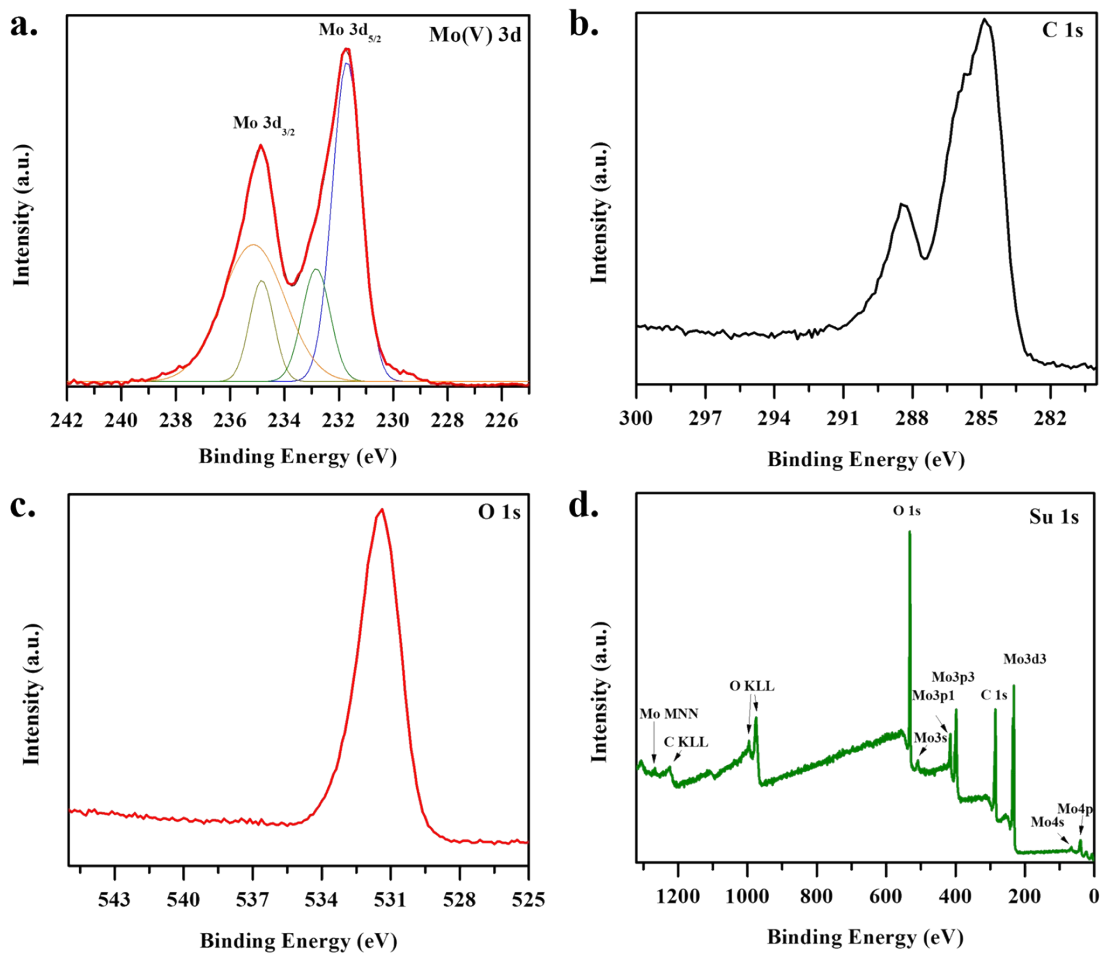


Figure S1. X-ray photoelectron spectra of BVR-107. a. Mo 3d, b. C 1s, c. O 1s, and d. the survey spectrum.

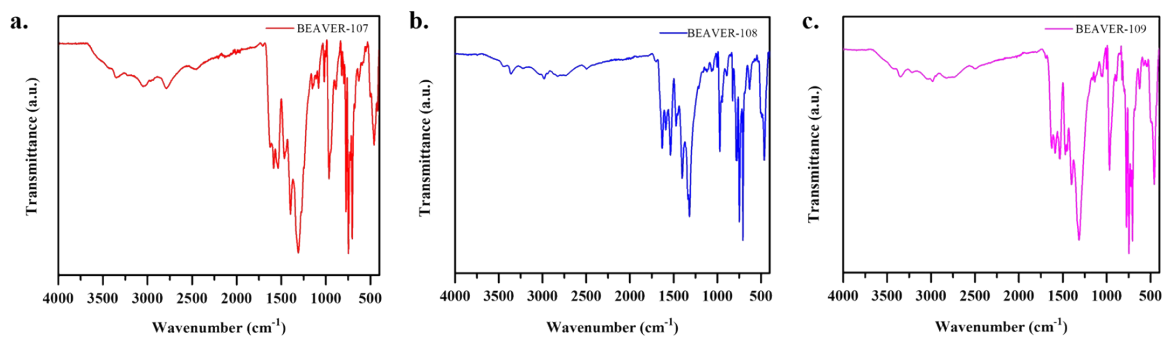


Figure S2. Fourier transform infrared spectra of solid a. BVR-107, b. BVR-108, and c. BVR-109.

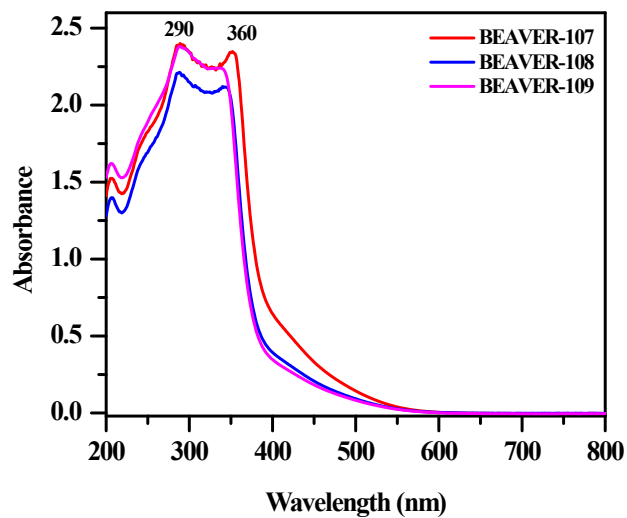


Figure S3. Ultraviolet-visible spectra of aqueous solutions of BVR-107, BVR-108, and BVR-109.

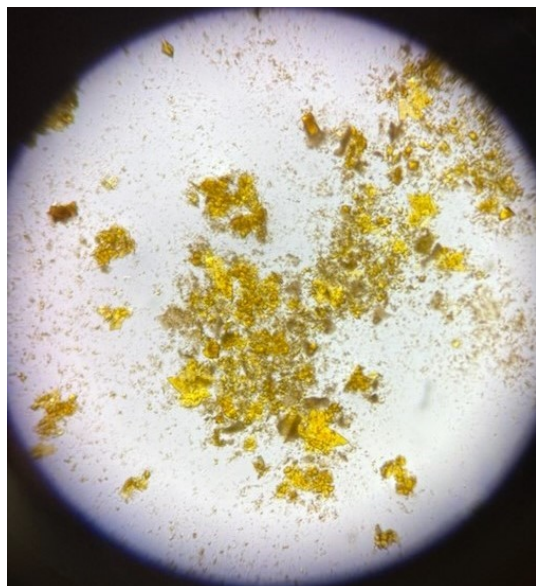


Figure S4. A visible-light microscopic image of a sample of the mixture of deep yellow crystals of BVR-108 and pale yellow crystals of BVR-109 crystallized in the same vessel.

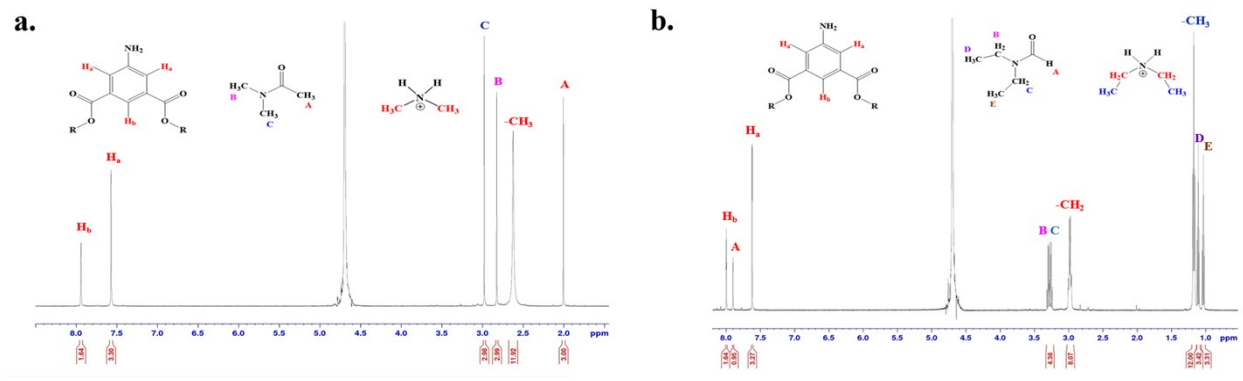


Figure S5. Solution ^1H NMR spectra of a. BVR-107 and b. BVR-108 dissolved in D_2O .

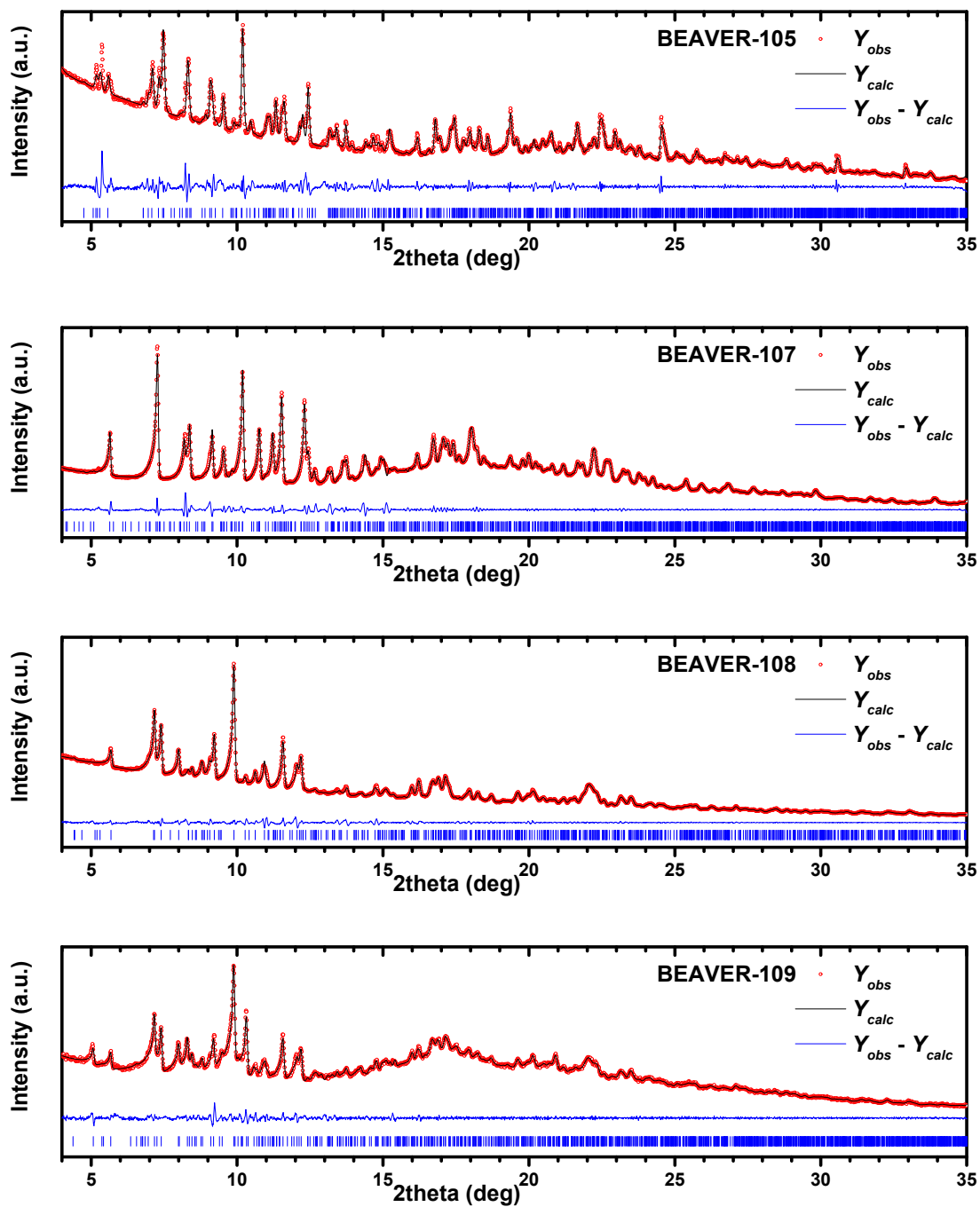


Figure S6. Pawley refinements of the PXRD patterns for bulk Mo(V)-MOP phases.

Table S1. Results of Pawley refinements for bulk Mo(V)-MOP phases.

	BVR-105	BVR-107	BVR-108	BVR-109
Space group	$P\bar{1}$	$Pmmm$	$P\bar{1}$	$P\bar{1}$
a [Å]	24.48357	38.52851	22.43329	18.10739
b [Å]	20.18912	25.25547	21.35463	25.42894
c [Å]	25.34534	39.94536	23.18887	27.34858
α [°]	107.35456	90	65.0565	100.12751
β [°]	86.79881	90	114.47693	102.39127
γ [°]	105.52957	90	111.12051	97.56231
Volume [Å ³]	11517.439	38869.048	8932.458	11918.456
Zero shift [°]	0.02078	0.0184	0.00894	0.0086
R_{wp}	3.43876	2.35947	2.26977	2.24859
R_{exp}	0.84482	0.5536	0.92962	1.21695
R_p	2.23157	1.38615	1.56384	1.59413
G.o.f.	4.07039	4.26205	2.44161	1.84772

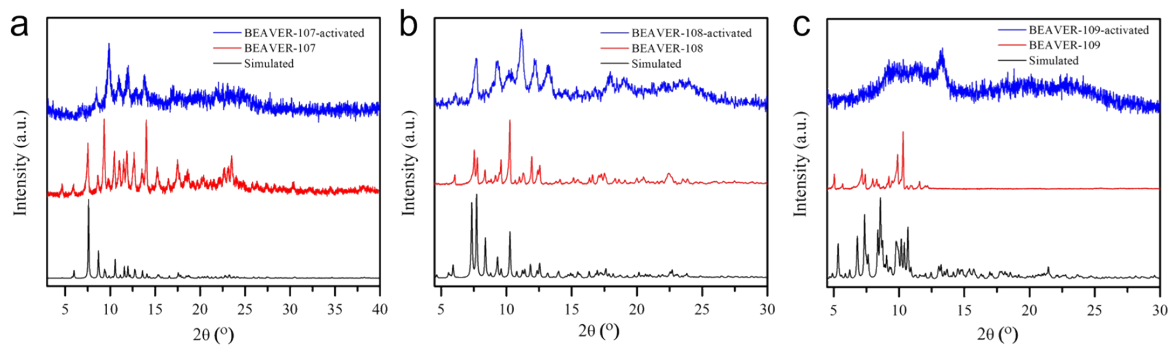


Figure S7. PXRD patterns of activated BVR-107, BVR-108, and BVR-109 compared to their as-made forms.

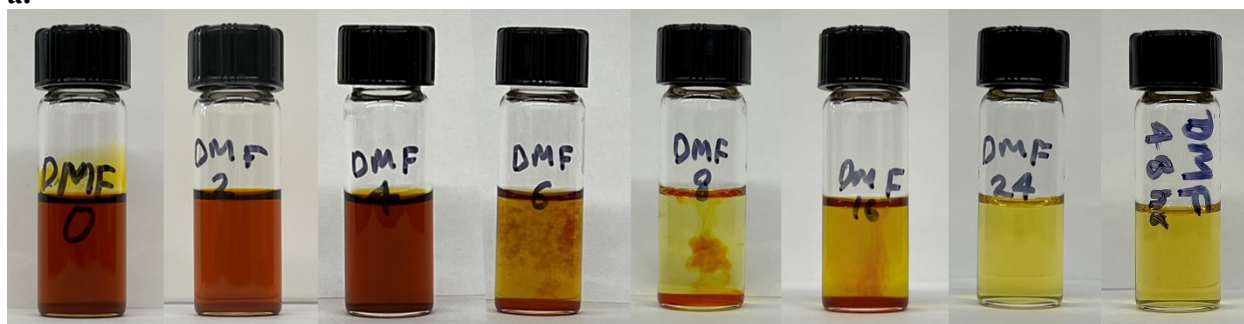
Table S2. Pseudofirst- and second-order rate constants k_1 and k_2 of amide hydrolysis in acidic and basic conditions.

Amide	Hydrolyzing agent		Temperature [°C]	$10^4 k_1$ [s ⁻¹]	$10^4 k_2$ [L·mol ⁻¹ ·s ⁻¹]	Ref.
	Name	Concentration [mol·L ⁻¹]				
DMF (95 vol%)	NaOH	0.02	25	2.08	.	12
			25	2.30	.	
DMF	NaOH	2	25	11	.	13
DMF	HClO ₄	0.1–1.5	70	.	1.80	14
			72	.	2.05	
			80	.	3.92	
			90	.	7.55	
	NaOH	0.02–0.5	70	.	51.9	
			72	.	58.6	
			80	.	96.6	
			90	.	171	
DMA	HCl	0.1	65	.	0.259	15
			75	.	0.654	
			85	.	1.39	
DMA	NaOH	.	25	.	11.0±0.5	16
			45	.	39.8	
			45	.	37.4	
			35	.	20.4	
			25	.	9.8	
			25	.	6.1	
DMA	NaOH	0.6–0.9	60	.	0.173	17
			65	.	0.238	
			70	.	0.335	
			75	.	0.477	
DMA	HClO ₄	.	80	0.887	.	18
			80	0.745	.	
			80	0.630	.	
			80	0.553	.	
			80	0.403	.	
			80	0.353	.	

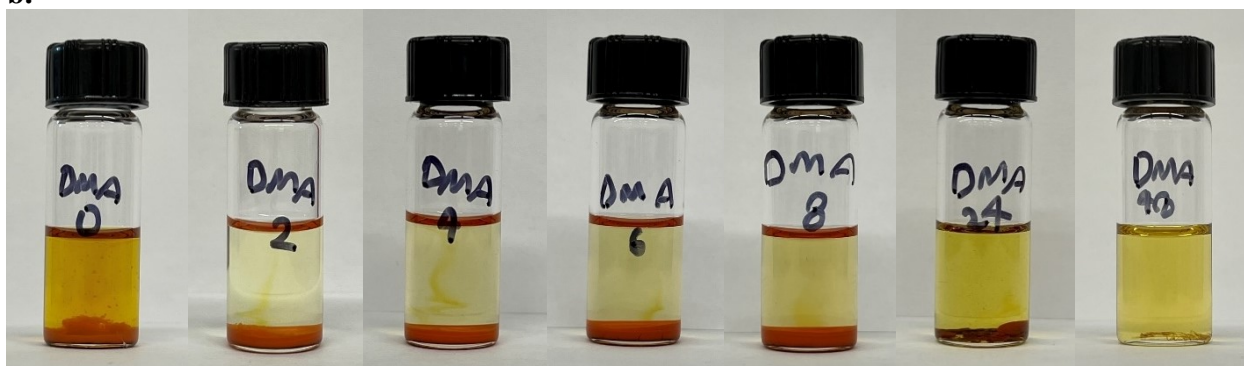
Table S3. Solubilities of metal–organic polyhedra.

	Solubility [g/L]				Ref.
	in H ₂ O	in MeOH	in DMSO	in DMF	
ZrMOP	0.0083(8)	1.5(3)	0.79(11)	0.012(3)	19
ZrMOP-ben	0.00176(18)	0.55(4)	1.1(2)	0.184(8)	19
ZrMOP-vb	0.0024(4)	1.3(7)	2.3(3)	0.47(4)	19
ZrMOP-tfmb	0.00171(11)	0.69(11)	0.95(5)	0.39(16)	19
Na ₆ H ₁₈ [Cu ₂₄ (5-hydroxy-1,3-benzenedicarboxylate) ₂₄]	110			6.49(19)	20, 21
(Pd(en)) ₆ (2,4,6-tri(4-pyridyl)-1,3,5-triazine) ₄			68(2)		21
Fe ₄ (4,4'-diaminobiphenyl-2,2'-disulfonate) ₆	340		3.101(11)		21, 22
BVR-107	4.30(2)				This work
BVR-108	10.25(7)				This work
BVR-109	14.41(10)				This work

a.



b.



c.

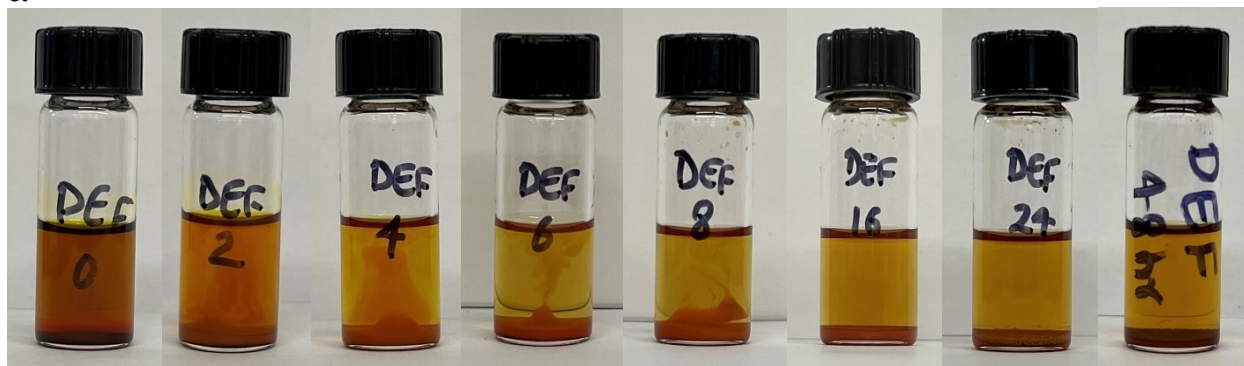


Figure S8. Photographs of vials containing the starting materials for the synthesis of a. BVR-105, b. BVR-107, c. BVR-108 (except for MeOH, see the Experimental section for details) taken after the number of hours of heating at 120 °C marked on each vial.

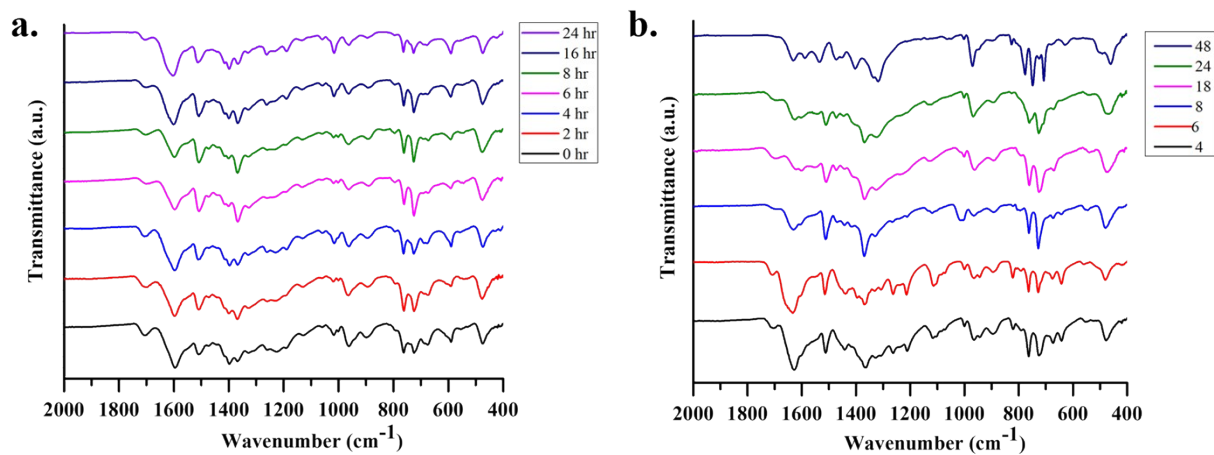


Figure S9. Fourier transform infrared spectra recorded on the reaction mixtures leading to the Mo(V)-MOP solvatomorphs. The reactions were run at 120 °C for given amount of time without the addition of MeOH to avoid precipitation. a. BVR-107. b. BVR-108.

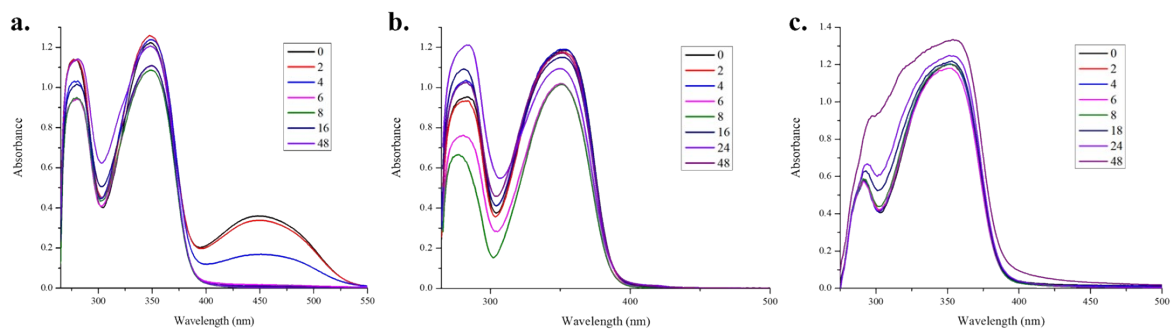


Figure S10. Ultraviolet-visible spectra recorded on the reaction mixtures leading to the Mo(V)-MOP solvatomorphs. The reactions were run at 120 °C for given amount of time without the addition of MeOH to avoid precipitation. a. BVR-105. b. BVR-107. c. BVR-108.

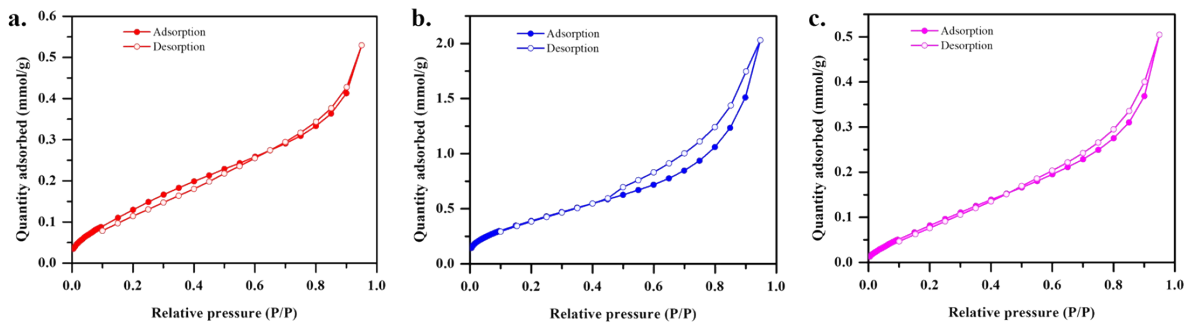


Figure S11. Sorption data for a. BVR-107, b. BVR-108, and c. BVR-109.

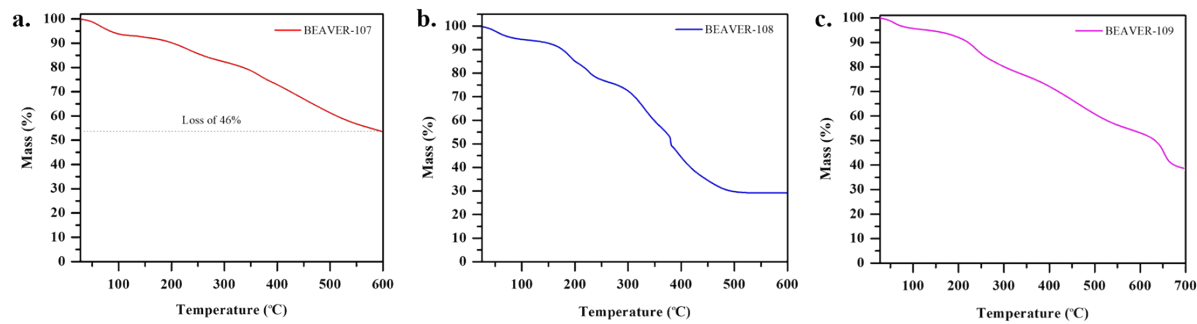


Figure S12. Thermogravimetric analyses of a. BVR-107, b. BVR-108, and c. BVR-109.

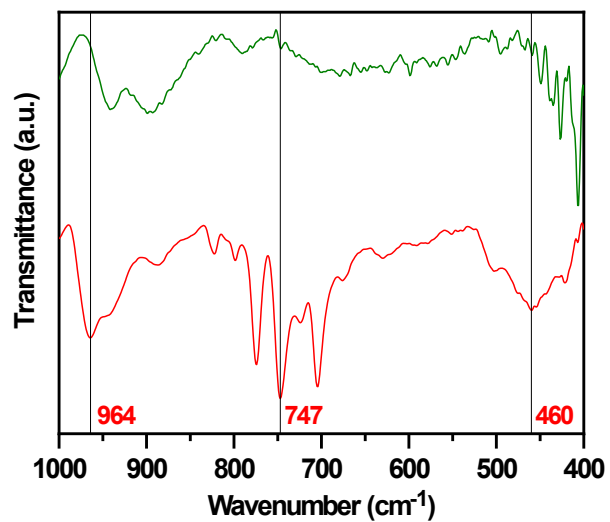


Figure S13. Fourier transform infrared spectra of solid BVR-107 a. as-made (red plots), and b. exposed to 600 °C (green plots).

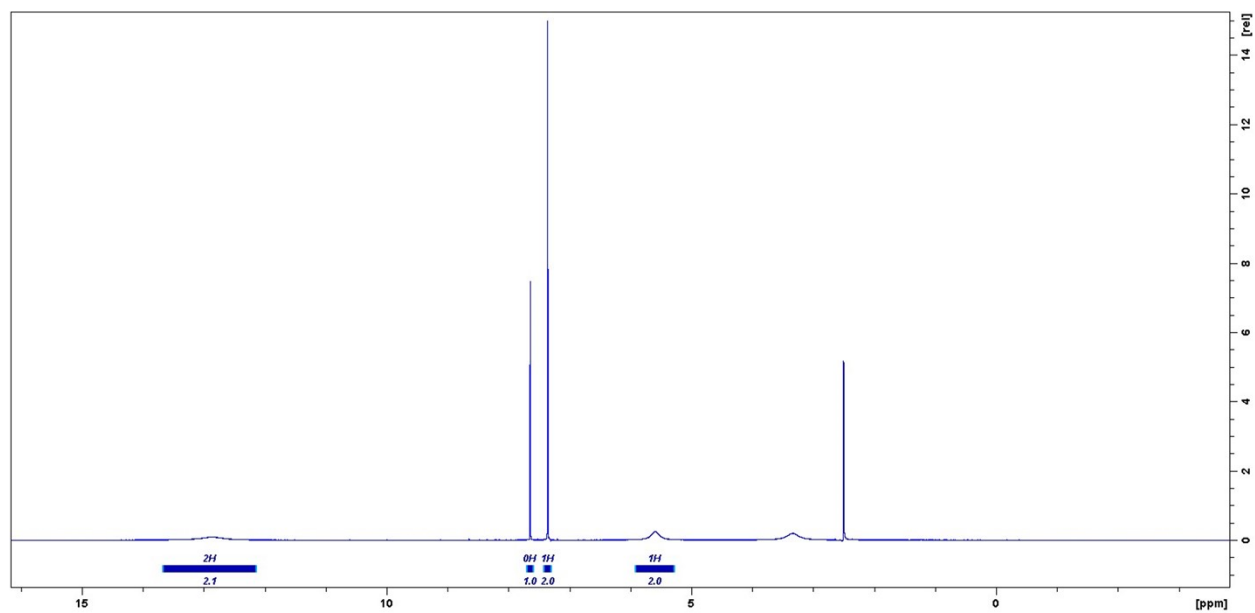


Figure S14. ¹H NMR spectrum of free H₂Iso-NH₂.

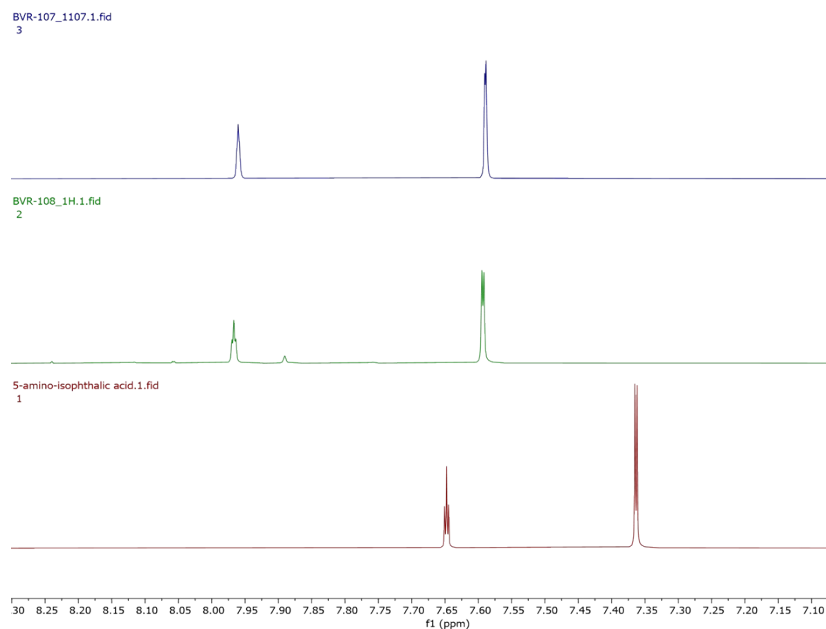


Figure S15. Comparison between the aromatic regions of the solution ¹H NMR spectra of BVR-107, BVR-108, and free H₂Iso-NH₂.

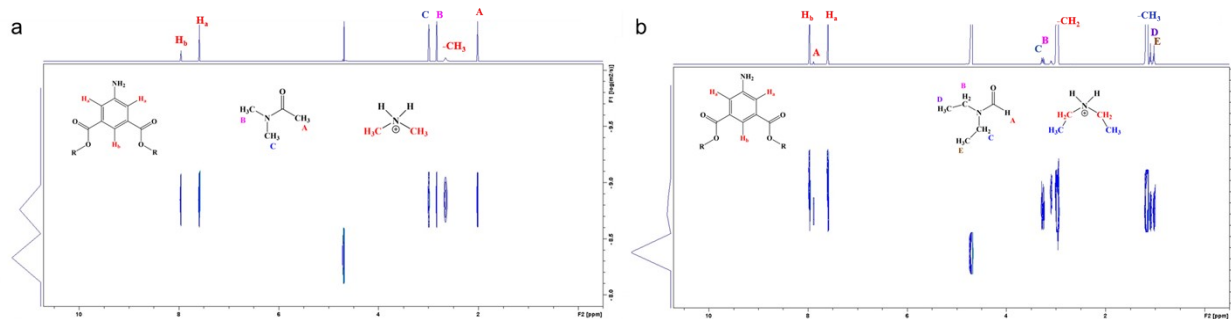


Figure S16. DOSY spectra of the BEAVER-107 and BEAVER-108 MOPs.

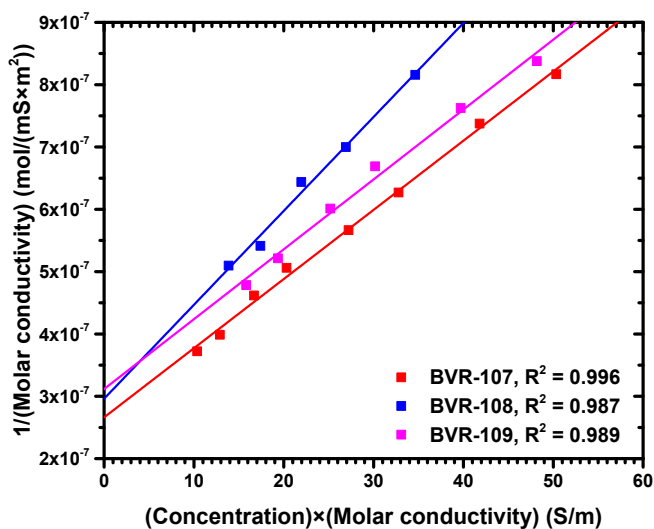


Figure S17. Fitting the concentration and molar conductivity data to Ostwald's dilution law. The intercept at zero concentration outputs the inverse of limiting molar conductivity, while the slope outputs the inverse of limiting molar conductivity squared multiplied by K_a ; both values are reported in Table 2.

References

1. O. V. Dolomanov, L. J. Bourhis, R. J. Gildea, J. A. K. Howard and H. Puschmann, *J. Appl. Crystallogr.*, 2009, **42**, 339-341.
2. G. Sheldrick, *Acta Crystallogr. A*, 2015, **71**, 3-8.
3. G. Sheldrick, *Acta Crystallogr. C*, 2015, **71**, 3-8.
4. A. Spek, *Acta Crystallogr. C*, 2015, **71**, 9-18.
5. S. A. Moggach, T. D. Bennett and A. K. Cheetham, *Angew. Chem. Int. Ed.*, 2009, **48**, 7087-7089.
6. A. Coelho, *J. Appl. Crystallogr.*, 2018, **51**, 210-218.
7. G. Kresse and J. Furthmüller, *Comput. Mater. Sci.*, 1996, **6**, 15-50.
8. J. P. Perdew, K. Burke and M. Ernzerhof, *Phys. Rev. Lett.*, 1996, **77**, 3865-3868.
9. S. Grimme, J. Antony, S. Ehrlich and H. Krieg, *J. Chem. Phys.*, 2010, **132**, 154104.
10. S. L. Dudarev, G. A. Botton, S. Y. Savrasov, C. J. Humphreys and A. P. Sutton, *Phys. Rev. B*, 1998, **57**, 1505-1509.
11. A. Jain, G. Hautier, S. P. Ong, C. J. Moore, C. C. Fischer, K. A. Persson and G. Ceder, *Phys. Rev. B*, 2011, **84**, 045115.
12. E. Buncel and E. A. Symons, *J. Chem. Soc. D: Chem. Commun.*, 1970, DOI: 10.1039/C29700000164, 164-165.
13. W. C. Cooper, A. Chilukoorie, S. Polam, D. Scott and F. Wiseman, *J. Phys. Org. Chem.*, 2017, **30**, e3701.
14. S. Langlois and A. Broche, *Bull. Soc. Chim. Fr.*, 1964, 812-816.
15. P. Bolton, *Aust. J. Chem.*, 1966, **19**, 1013-1021.
16. R. J. Washkuhn and J. R. Robinson, *J. Pharm. Sci.*, 1971, **60**, 1168-1175.
17. U. Mazzucato, A. Foffani and G. Cauzzo, *Ann. Chim.*, 1960, **50**, 521-529.
18. T. Yamana, Y. Mizukami, A. Tsuji and M. Ikuta, *Chem. Pharm. Bull.*, 1972, **20**, 1778-1784.
19. M. G. Sullivan, G. E. Sokolow, E. T. Jensen, M. R. Crawley, S. N. MacMillan and T. R. Cook, *Dalton Trans.*, 2023, **52**, 338-346.
20. J. Liu, C. R. P. Fulong, L. Hu, L. Huang, G. Zhang, T. R. Cook and H. Lin, *J. Membr. Sci.*, 2020, **606**, 118122.
21. C. R. P. Fulong, J. Liu, V. J. Pastore, H. Lin and T. R. Cook, *Dalton Trans.*, 2018, **47**, 7905-7915.
22. P. Mal, D. Schultz, K. Beyeh, K. Rissanen and J. R. Nitschke, *Angew. Chem. Int. Ed.*, 2008, **47**, 8297-8301.